agriculture

MDPI

Article

Microclimate and Plant Transpiration of Tomato (*Solanum lycopersicum* L.) in a Sunken Solar Greenhouse in North China

Li Yang [1], Haijun Liu [1,*], Shabtai Cohen [2] and Zhuangzhuang Gao [1]

[1] Beijing Key Laboratory of Urban Hydrological Cycle and Sponge City Technology, College of Water Sciences, Beijing Normal University, Beijing 100875, China; 201921470027@mail.bnu.edu.cn (L.Y.); bnugaozz@mail.bnu.edu.cn (Z.G.)
[2] Institute of Soil, Water and Environmental Sciences, Agricultural Research Organization, The Volcani Centre, P.O. Box 15159, Rishon LeZion 7505101, Israel; vwshep@volcani.agri.gov.il
* Correspondence: shanxilhj@bnu.edu.cn; Tel.: +86-136-8133-4108

Abstract: The solar greenhouse is a common protected structure for crop production when ambient temperatures are low. In the North China Plain (NCP) winter temperatures are very low and an improved solar greenhouse with a lowered soil surface (0.5–1.5 m deep), referred to as a sunken solar greenhouse (SSG), is used. A four-season experiment was conducted in a commercial SSG with tomato crops to characterize internal microclimate, sap flow (SF) and crop coefficients. Results show that temperature inside the SSG could be more than 20 °C higher than outside in winter, which favors tomato growth and resulted in acceptable yields. Daily total SF was related to solar radiation, vapor pressure deficit (VPD) and temperature, in that order, both in winter and summer. The decoupling coefficient (which is the ratio of radiative to aerodynamic influences on evapotranspiration) in daytime was 0.76 in winter and 0.84 in summer, indicating strong decoupling (i.e., predominance of radiative influences) of the internal environment where wind speed was low. Basal crop coefficients at the mid stage of crop growth averaged 1.15–1.43 in winter and 0.91–0.92 in spring and summer. Thus, in the SSG, for similar climatic conditions sap flow in winter was higher than that in summer, which should be considered in irrigation scheduling.

Keywords: air temperature; sap flow; crop coefficient; irrigation efficiency; evapotranspiration

Citation: Yang, L.; Liu, H.; Cohen, S.; Gao, Z. Microclimate and Plant Transpiration of Tomato (*Solanum lycopersicum* L.) in a Sunken Solar Greenhouse in North China. *Agriculture* **2022**, *12*, 260. https://doi.org/10.3390/agriculture12020260

Academic Editors: Jiandong Wang and Yanqun Zhang

Received: 17 December 2021
Accepted: 4 February 2022
Published: 11 February 2022

1. Introduction

Greenhouses are widely used to cultivate offseason cash crops in order to obtain higher yields than in open cropping systems [1–3]. In China, greenhouse area is steadily increasing. In 2018 it was 196.4 million hectares, 2.4 times that in 2008 [4]. Vegetable production in these greenhouses accounted for approximately 30% of China's total vegetable production [4]. The North China Plain (NCP) is one of the main food and vegetable production regions in China, and there, vegetable production in greenhouses is popular due to the low winter temperatures [5,6]. Recently, an improved solar greenhouse was introduced there, with a soil surface 0.5–1.5 m lower than the outside surface, which increases inside air and soil temperatures and improves crop growth in winter [7]. This greenhouse is referred to as a sunken solar greenhouse (SSG). The minimum temperature increases with greenhouse surface depth in the SSG [8]. Because the SSG does not need extra heating and is maintained the same way as a traditional solar greenhouse, SSG popularity has been increasing in NCP.

Microclimate inside the greenhouse is critical for crop growth [9,10] and has been widely investigated [11–15]. Increased air temperatures inside passive, solar heated greenhouses in the winter period in North China are favorable for crop growth [16]. However, the temperature inside the greenhouse can reach 50 °C in summer in central China [17] which is detrimental. This extra high inside temperature in summer can be attenuated by

shading and ventilation [18–20]. Ahemd et al. [21] reported in a review paper that combining a shading method with ventilation could efficiently improve overall microclimate in sunny regions. However, in cold regions shading reduces heat loss from the greenhouse at night and can maintain temperatures 5 °C higher than outside, thus saving approximately 15–20% of the energy used for heating. Internal relative humidity is always higher than that outside because of the poor ventilation [12,22]. Inside short wave radiation is always lower than that outside due to the transmission of cover materials. The transmissivity of the greenhouse, defined as the ratio of inside short wave radiation to the corresponding outside short wave radiation, ranged from 30% to 95% depending on the cover materials, service time and greenhouse structure [14,23,24]. In the NCP, transparent plastic films are always used to cover the greenhouses, and the transmissivity was reported to be 0.6–0.7 [22,25].

Inside plant transpiration is closely related to inside microclimate. Generally, it is reported that transpiration rate is positively related to inside radiation, temperature and vapor pressure deficit (VPD). Gong et al. [26] found that the correlation coefficients of greenhouse tomato evapotranspiration (ET_c) with radiation, temperature and VPD were all greater than 0.6. Mao et al. [27] also reported that the correlation coefficients of plant sap flow with radiation, temperature and VPD of greenhouse tomatoes on sunny days were greater than 0.6. Under most cases, inside plant transpiration is not closely related to inside wind speed because the wind speed is very low (<0.2 m s^{-1}) [28–30].

Sap flow methods are widely used to investigate transpiration of plants assuming that the change of water storage in the plant is negligible relative to the daily water flux. Thus, on a daily scale, total sap flow (SF) equals plant transpiration [31,32]. Therefore, SF data are useful for irrigation scheduling and evaluating water use efficiency.

Tomato is one of the favorite vegetables in China, and widely cultivated in greenhouses [33–35]. Farmers in the NCP often cultivate tomato plants according to their previous experience with outdoor cultivation. Thus, irrigation rates always exceed plant requirements, leading to low water use efficiency [36,37]. Excessive irrigation in this region may intensify the water shortage problem in the NCP, which has only 8% of the national water resources but produces more than 30% of the national grain yield [38].

Tomato is very vulnerable to high temperature and water stress [33,39–42]. Sato et al. [40] showed that when the temperature was 32/26 °C in day/night, one variety had 20% less fruit set compared to 28/22 °C, while fruit set for other varieties approached zero (between 1.8% and 0). Ghorbanpour et al. [43] treated 30-day-old tomato plants to 8 °C for 6 days and found that the plants suffered from low temperature stress, which had an impact on plant growth, ion leakage, leaf relative water content and quantum yield. Optimal microclimate would enhance tomato growth and yield production. Therefore, experiment-based knowledge is important for farmers, including appropriate irrigation rates, when crops are cultivated in this new type of greenhouse.

The objectives of this study were to (1) investigate microclimate, (2) analyze the sap flow and its response to microclimate, and (3) determine the crop coefficient in winter, spring and summer seasons in this new type of greenhouse.

2. Materials and Methods

2.1. Experimental Site

A four-season experiment, from September 2018 to January 2020, was conducted in a commercial solar greenhouse at the Dacaozhuang National Breeding Experimental Station in Ningjin County, Hebei Province, China (37°30′6″ N; 114°57′22″ E). Mean annual precipitation is 430 mm, with 60% from July to September; annual mean temperature is 13 °C and the frost-free period is about 200 d. The CO_2 level inside the greenhouse was approximately 500 μmol mol^{-1}. The soil texture in the 0–40 cm depth was silty loam [44]. In the upper 40 cm soil layer the mean soil bulk density was 1.40 g cm^{-3}, field capacity was 0.40 cm^3 cm^{-3} and wilting point was 0.22 cm^3 cm^{-3}. The measured nitrate nitrogen content in the upper 40 cm soil layer before this experiment was 29.81 mg kg^{-1}, available potassium content 150.5 mg kg^{-1}, and available phosphorus 7.02 mg kg^{-1}.

Photos of the sunken solar greenhouse (SSG) are shown in Figure 1. It had a soil surface 1 m lower than that outside. This structure impedes heat exchange from outside and keeps the inside warm, which is critical for offseason winter crop cultivation in the NCP. The greenhouse was 166 m long in the east-west direction and 10 m wide, covering an area of 1660 m^2. The sun is on the south side of the greenhouse aiming to collect as much solar radiation as possible. The northern wall is designed to store heat from solar heating. It was 1.2 m thick at the top and 5 m at the bottom. The greenhouse was clad with a 0.1 mm- thick transparent polyethylene film. A rolled straw curtain was used to cover the top of the greenhouse at night in winter to reduce convective heat loss. There is a vent on the top of the greenhouse near the north wall for natural ventilation. When the inside temperature exceeds 25 °C, the vent is manually opened. The vent was usually opened at noon in the winter for approximately 1–2 h, and was normally open all day in spring and summer. The vent was opened approximately 20 cm in the autumn and winter seasons and 80 cm in the spring and summer seasons.

Figure 1. Photos of the sunken solar greenhouse. (**a**) Inside view during tomato planting. (**b**) A view of the sunken soil inside. (**c**) Outside view in winter. The front plastic cover faces south, and the rolled straw cushion is on the top of the roof.

Tomatoes (*Solanum lycopersicum* L., variety Jinfenshuoguo) were planted in four seasons, 2018 autumn–winter season (September 2018–January 2019), 2019 spring season (January 2019–June 2019), 2019 summer season (June 2019–August 2019) and 2019 autumn–winter (August 2019–January 2020), referred to as 2018AW (Autumn–Winter), 2019SP (Spring), 2019SU (Summer) and 2019AW, respectively. The tomato seedlings were transplanted when they had four leaves, corresponding to 26–day–old seedlings in spring and summer, and 30 days in autumn and winter.

In the soil, single ridge and double row planting systems were used. Each ridge was 9 m long, 1 m wide and 0.15–0.2 m high. The distance between ridges was 0.4 m, used for plant management and tomato harvest. The distance between rows on each ridge was 0.5 m, and the spacing between plants was 0.4 m, which yielded an average density of 3.6 plants per m^2.

Under normal management, tomato plants were grown naturally until height was approximately 170 cm and the fifth branch fruits were flowering, after which the stems above the fifth branch were trimmed. This practice suppresses apical dominance, improves ventilation of the lower part of the plant, and reduces transpiration and nutrient requirements. Further leaves in the lower part of the stem were trimmed at the later growth stage to enhance fruit growth.

2.2. Irrigation and Fertilization

Irrigation was applied by drip. Drip laterals (Hebei Runtian Water-Saving Equipment Co., Ltd., Shijiazhuang, China) were parallel to the crop row, with one lateral (16 mm in diameter) per row. Dripper spacing was 40 cm (one dripper per plant), and dripper discharge 2.5 L h^{-1} under the working pressure of 0.1 MPa. An underground reservoir of approximately 10 m^3 inside the SSG was used for irrigation. A filter, water meter and pressure meter were deployed in the head of the drip irrigation system to control working pressure and record irrigation water amount.

Fertilizer application included base and topdressing fertilizer. The base fertilizer was compound fertilizer with nutrient ratios of N:P_2O_5:K_2O being 15:15:15 (Lomon Land Agriculture Co., Ltd., Mianzhu, China). The topdressing fertilizer used was soluble. In the 2018AW season, the nutrient proportions for the topdressing fertilizer were 15:5:35 (Lomon Land Agriculture Co., Ltd., Mianzhu, China) for N:P_2O_5:K_2O, and in the 2019SU and 2019AW seasons 20:20:20 (Hong Sifang Co., Ltd., Hefei, China). Both soluble fertilizers used in the other three seasons were applied in the 2019SP season. Topdressing fertilizers were applied with the irrigation water as fertigation.

At the outset, irrigation and fertilizer application were carried out by the farmer according to local practice. In the first season, irrigation began when the farmer found that leaf emergence was weak and the growth rates of plant and fruit slowed down. This local irrigation practice resulted in much higher soil water potential and consequently the irrigation efficiency (IE), the ratio of crop evapotranspiration to irrigation amount, was low (0.31). In the following three seasons, we installed three dial type tensiometers (Beijing Waterstar Tech Co., Ltd., Beijing, China) at 20 cm depth under the drip tape to help the farmer schedule irrigation [45–47]. When soil matric potential reached −35 kPa irrigation was started.

Total fertilizer application in the four seasons is summarized in Table 1. Nitrogen and potassium were applied according to local practice. Because of the low level of available phosphorus in root zone before the experiment (7.02 mg kg^{-1}), supplemental phosphorus fertilizer was applied. Granular compound fertilizer was spread and mixed with soil during soil tillage and soluble compound fertilizer was applied as topdressing fertilization during the growing season using a Venturi system deployed in the main pipe. The irrigation amount, irrigation events and reference crop evapotranspiration (ET_o) are shown in Table 2. In the 2019SU season, tomato plants in the flowering and fruit-setting period in later August suffered from disease and heat stress and few fruits were harvested. Therefore, the farmer aborted the crop, i.e., reduced the irrigation and fertilization and removed all tomato plants before the time of the normal harvest in order to prepare for the following tomato season.

Table 1. Growth period and fertilization amounts in each season.

Planting Season	Growth Period	Fertilization	N (kg ha^{-1})	P_2O_5 (kg ha^{-1})	K_2O (kg ha^{-1})
Autumn–Winter (2018AW)	September 2018–January 2019	Base fertilizer	114	114	114
		Topdressing fertilizer	68	23	159
		Total	182	137	273
Spring (2019SP)	January 2019–June 2019	Base fertilizer	157	157	157
		Topdressing fertilizer	110	78	172
		Total	267	235	329
Summer (2019SU)	June 2019–August 2019	Base fertilizer	81	81	81
		Topdressing fertilizer	22	22	22
		Total	103	103	103
Autumn–Winter (2019AW)	August 2019–January 2020	Base fertilizer	114	114	114
		Topdressing fertilizer	91	91	91
		Total	205	205	205

Table 2. Irrigation amount, irrigation events and inside reference crop evapotranspiration (ET_o) during the four experimental periods.

Planting Season	Total Irrigation Depth (mm) *	Sap Flow Measurement Period **			
		ET_o (mm)	Irrigation Depth (mm)	Irrigation Events	Irrigation Depth per Time (mm)
2018AW	516	64.1	255	6	42.5
2019SP	491	184.0	265	8	33.1
2019SU	199	101.3	31	2	15.5
2019AW	508	74.3	162	6	27.0

Note: * Total irrigation depth is the sum of irrigation amount in each growth season, from the seedling transplanting to the last irrigation event in an experimental season. ** The data in the columns of ET_o, irrigation depth, irrigation events and irrigation depth per time were only recorded in the sap flow measurement period. Sap flow was measured in 2018AW from 1 November 2018 to 16 January 2019, in 2019SP from 17 April 2019 to 10 June 2019, in 2019 SU from 10 July 2019 to 13 August 2019, and in 2019AW from 27 October 2019 to 5 January 2020.

2.3. Plant Growth and Yield Measurements

Plant height and leaf area were measured once a month. At the first measurement, three representative plants were labeled and used for the rest of the season. Leaf area was determined by measuring the maximum length and width of each large stalk leaf. A relationship between leaf area and leaf width and length was derived from measurements on 11 leaves. Individual leaf area was measured using a leaf area meter (Model LI-3000C, LI-COR Biosciences, Lincoln, NE, USA). The fitting result is $A = 0.37\ L \times W$ with $R^2 = 0.92$ ($N = 11$), where A is the area of a leaf (cm^2), and L and W are leaf length and width, respectively (cm). Leaf area index (LAI) was calculated using the mean leaf area per plant and the soil surface (S, in cm^2) covered by a plant, i.e., $LAI = \Sigma A/S$.

Marketable fresh tomato yield in the SSG was recorded at each sale date. The seasonal yield was the sum of all sales in a season.

2.4. Sap Flow Measurement

Eight representative plants with similar growth parameters were selected in the middle of the experimental site. One set of sap flow gauges (Flow32-1K, Campbell Scientific, Logan, UT, USA) was installed on each selected plant approximately 15 cm above the ground surface. The measurement period was from flowering and fruit expansion to ripening when plants were big enough for sensor installation and crop evapotranspiration was high. All sap flow data were sampled at 1 min intervals and 30 min means were recorded with a CR1000 datalogger (Campbell Scientific, Logan, UT, USA). Data were regularly downloaded for sap flow calculation and data analysis.

2.5. Stomatal Conductance Measurement

Stomatal conductance (g_s) was measured in the middle growth period in the last two seasons using an LI-6800 portable photosynthesis system (LI-COR Biosciences, Lincoln, NE, USA). The first fully grown leaf from the top of the plant was selected. Three leaves from each of three different plants were selected and the mean value was used for data analysis. Measurements were made hourly from 8:00 to 18:00 on 15 July in the 2019SU season, and 11:00 to 16:00 on 21–22 December 2019 in the 2019AW season. The short measurement period on 21–22 December 2019 was because the SSG must be covered by a straw curtain approximately one hour before sunset to reduce heat loss. During the measurement, the environmental conditions in the LI-6800 system tracked the microclimate conditions in the greenhouse, except for the CO_2 concentration in the sample chamber, which was set to 400 $\mu mol\ mol^{-1}$ to reduce the effect of the CO_2 variations caused by top vent opening and closing on measured stomatal conductance.

2.6. Meteorological and Soil Physical Parameters

Meteorological parameters were measured with a meteorological station deployed in the middle of the greenhouse. The measured variables included total solar radiation (Model TBQ-2, Jinzhou Sunshine Technology Co., Ltd., Jinzhou, China), soil heat flux density (HF-1, Jinzhou Sunshine Technology Co., Ltd., Jinzhou, China), air temperature, relative humidity (Model VP-4, METER Group, Inc., Pullman, WA, USA) and air velocity (two-dimensional ultrasonic anemometer ATMOS 22, METER Group, Inc., Pullman, WA, USA) at 2 m height. Microclimate parameters were also measured with an automatic climate station in the experimental station. All data inside the SSG and at the experimental station were sampled at 1 min intervals and 30 min averages were stored.

Soil matric potential (Model MPS-6 sensor, METER Group, Inc., Pullman, WA, USA) at 20 cm depth was measured. Sensors were installed at 20 cm depth to measure soil matric potential in the four planting seasons. In order to give farmers access to soil moisture data three dial type tensiometers (Dial-type tensiometer, Beijing Waterstar Tech. Co., Ltd., Beijing, China) were installed in the SSG in the last three planting seasons. Soil temperatures (Model MPS-6 and 5TE, METER Group, Inc., Pullman, WA, USA) were measured at depths of 10, 20, 30 and 40 cm. The data measured by sensors were sampled at 1 min intervals and 30 min average were stored using an EM50 datalogger (METER Group, Inc., Pullman, WA, USA). Data from the manual tensiometer were manually recorded every day.

3. Theoretical Methods

3.1. Reference Crop Evapotranspiration

Hourly reference crop evapotranspiration ($ET_{o,hr}$) was calculated, and the daily ET_o was computed using the FAO 56 Penman–Monteith equation [48].

$$ET_{o,hr} = \frac{0.418\Delta(R_n - G) + \gamma(37/(T_{hr} + 273))u_2 VPD}{\Delta + \gamma(1 + 0.34\,u_2)} \quad (1)$$

where $ET_{o,hr}$ is hourly reference evapotranspiration (mm h^{-1}), R_n is hourly net radiation (MJ m^{-2} h^{-1}), G is hourly soil heat flux density (MJ m^{-2} h^{-1}), T_{hr} is hourly mean air temperature (°C), Δ is saturation slope of the saturation vapor pressure curve at T_{hr} (kPa $°C^{-1}$), γ is the psychrometric constant (kPa $°C^{-1}$), and u_2 is hourly mean air velocity at 2 m height (m s^{-1}).

Vapor pressure deficit, VPD (kPa), was computed as

$$VPD = 0.6108 \exp\left(\frac{17.27 T_{hr}}{T_{hr} + 237.3}\right)(1 - RH_{hr}/100) \quad (2)$$

where RH_{hr} is hourly mean relative humidity (%).

3.2. Decoupling Coefficient

The decoupling coefficient (Ω) describes the relative contributions of the radiative and aerodynamic terms to crop transpiration, as described by the Penman–Monteith equation. These terms are the right- and left-hand terms in the numerator of Equation (1) above. When plants are well irrigated and exposed to sunshine, low wind speed and high humidity transpiration is mainly controlled by solar radiation (i.e., decoupled), and Ω approaches 1 [23]. On the other hand, when transpiration is mainly driven by the vapor pressure deficit and wind velocity the contribution of aerodynamic term dominates (i.e., coupled conditions) and Ω tends to 0. The decoupling coefficient Ω was calculated using the following equation [49,50]:

$$\Omega = \frac{\Delta^* + \gamma}{\Delta^* + \gamma^*} \quad (3)$$

where Ω is the decoupling coefficient. For greenhouse conditions Δ* and γ* are defined as [50]:

$$\Delta^* = \Delta\left(1+\frac{r_b}{r_a}\right) \quad (4)$$

$$\gamma^* = \gamma\left(1+\frac{r_c + r_b}{r_a}\right) \quad (5)$$

where r_b is boundary layer resistance (s m^{-1}), r_a is aerodynamic resistance (s m^{-1}), r_c is canopy resistance (s m^{-1}).

Boundary layer resistance r_b was calculated as [51]:

$$r_b = \frac{305(D/u)^{0.5}}{LAI} \quad (6)$$

where D is the characteristic leaf dimension (m), u is wind speed at 2 m height (m s^{-1}) and LAI is the leaf area index.

The aerodynamic resistance r_a was calculated assuming neutral stability as [48]:

$$r_a = \ln\left[\frac{z_m - d}{z_{om}}\right] \ln\left[\frac{z_h - d}{z_{oh}}\right] k^{-2} u_2^{-1} \quad (7)$$

where z_m is the height of wind measurements (m); z_h is the height of humidity measurements (m); d is zero plane displacement height, taken as (2/3)h (m), h is crop height (m); z_{om} is roughness length governing momentum transfer, taken as 0.123 h (m); z_{oh} is roughness length governing transfer of heat and vapor, taken as $0.1z_{om}$ (m); k is von Karman's constant (=0.41) [48].

The canopy resistance r_c was calculated as [48]:

$$r_c = \frac{r_s}{LAI_{active}} = \frac{r_s}{0.5LAI} \quad (8)$$

where r_s is stomatal resistance of well illuminated leaves (s m^{-1}). In this study, we measured the stomatal conductance of the first fully grown leaf from the top of the plant, and r_s was calculated as the inverse of stomatal conductance. LAI_{active} is active leaf area index and is calculated as LAI_{active} = 0.5 LAI [48], where LAI is leaf area index.

3.3. Irrigation Efficiency

The irrigation efficiency (IE) is defined as the ratio of actual crop evapotranspiration (ET_a) to the irrigation amount (I) [52]. In this study, all the soil surface was covered with a plastic sheet to reduce weed growth and maintain a clean surface for fruit harvest. This cover also reduces soil evaporation to negligible amounts. Therefore, crop ET_a was assumed to be plant transpiration in this study. The IE was calculated using the following equation:

$$IE = ET_a/I \quad (9)$$

where ET_a is crop evapotranspiration (mm), equal to the sap flow in this study; I is irrigation depth (mm).

3.4. Statistical Analysis

All computations in this study were performed using a Microsoft Excel template, and all graphs in this study were created using Origin 2018 (OriginLab Co., Northampton, MA, USA). Statistical analyses were performed using SPSS 20.0 (IBM, New York, NY, USA) to calculate the correlation level between inside and outside microclimate.

4. Results

4.1. Irrigation and Soil Matric Potentials

Table 2 shows irrigation times and amounts during the sap flow measurement period in the four seasons. Total irrigation in the 2018AW, 2019SP and 2019AW seasons were similar and approximately 500 mm. In the 2019SU season, extremely high temperatures inside negatively influenced crop growth, so the farmer aborted the crop, i.e., stopped irrigation and finished the season in order to prepare for the following winter season, which resulted in the lowest irrigation amount (199 mm). During the middle growth stage in which crop growth is rapid and tomato fruits expand, the average total irrigation depth was 42.5 mm in the 2018AW season, decreased to 33.1 mm in the 2019SP season, and was 15.5–27.0 mm in the last two seasons. The decrease in irrigation depth with time is mainly due to the tensiometer application in the last three seasons. This practice resulted in an increase in the irrigation efficiency (IE) from 0.31 in 2018AW to approximately 0.6 in 2019SP and 2019AW seasons. The higher IE (3.03) in the 2019SU season was due to the low irrigation (Table 2) resulting from the farmer's premature abortion of the crop.

Figure 2 shows the soil matric potentials (SMPs) measured at 20 cm depth in the root zone. In most cases SMPs were higher than −35 kPa, a threshold for non-water-stress conditions [53]. In the 2018AW and 2019AW seasons, SMPs were generally higher than −35 kPa, indicating optimal soil water conditions for the tomato plants [53]. In the 2019 spring and summer seasons, most SMPs were higher than −50 kPa (Figure 2), which is also higher than the threshold of −50 kPa for tomato planted in an open field [54]. Therefore, we conclude that the tomato crop grew with sufficient soil water for most of the experimental period.

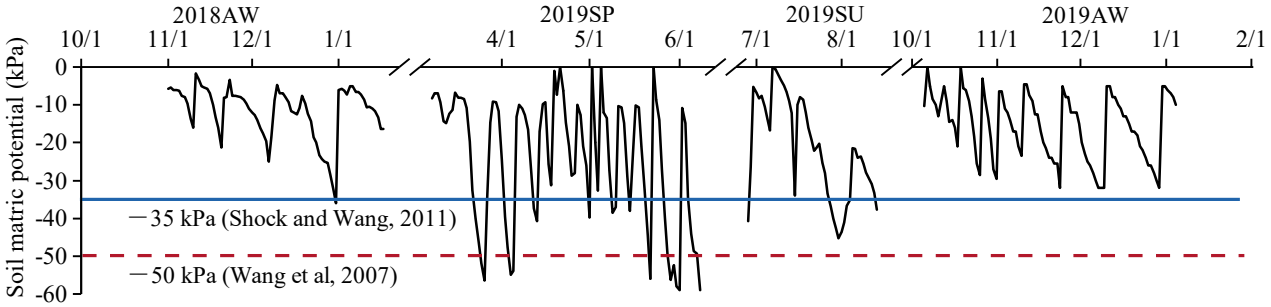

Figure 2. Changes of soil matric potential at 20 cm depth in the four seasons. Blue solid line and red dashed line, respectively, indicate thresholds of soil matric potentials of −35 and −50 kPa for tomato plants, proposed by [53,54].

4.2. Climate Inside and Outside the Sunken Greenhouse

The daily course and daily average values of climate variables observed inside and outside the greenhouse during the experimental period are shown in Figures 3 and 4, respectively. Generally, inside microclimate was strongly coupled to that outside. Linear relationships between inside and outside conditions are shown in Table 3. The inside wind velocity in the 2018AW season was not measured because of a sensor fault.

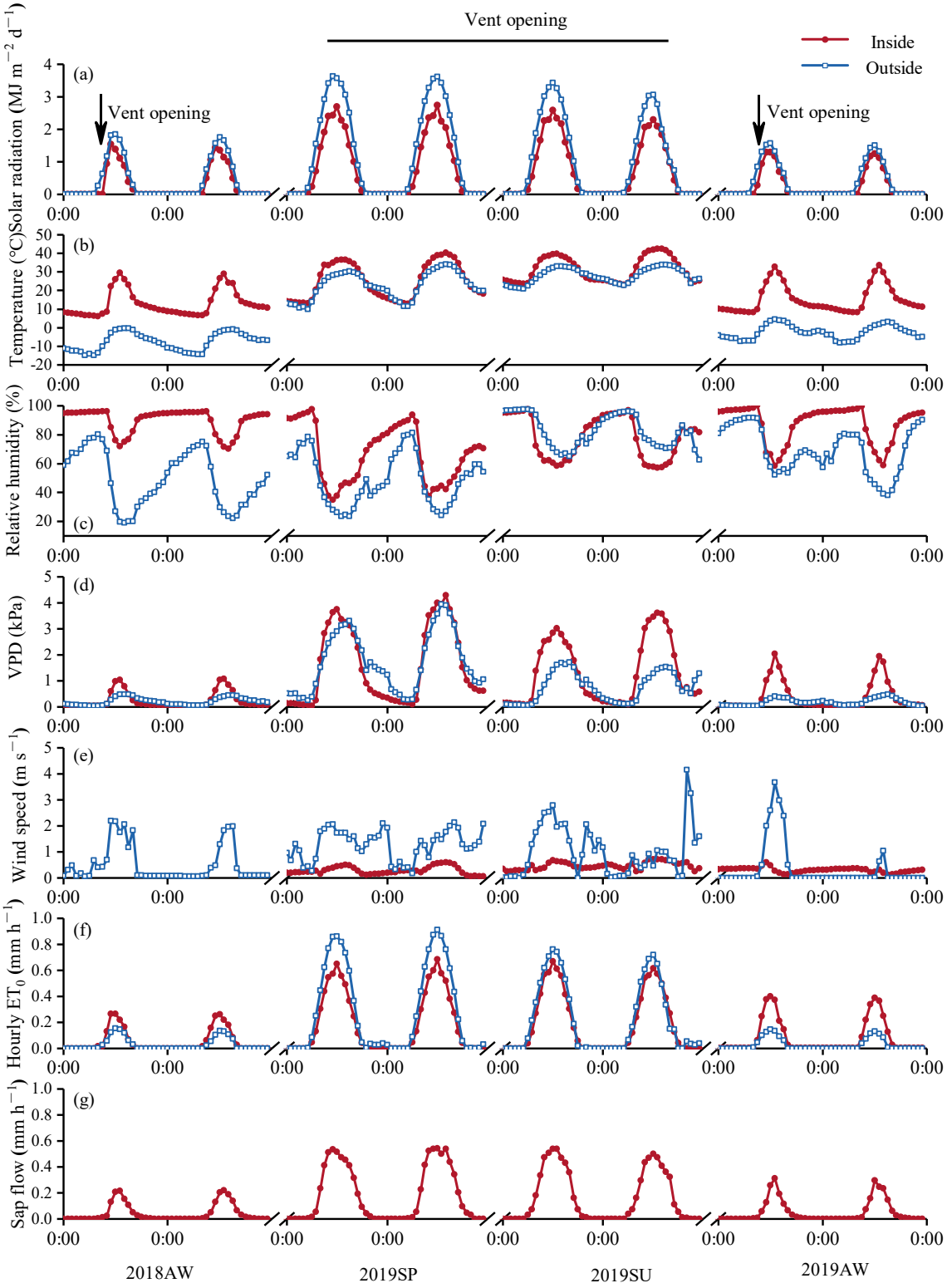

Figure 3. Daily courses of solar radiation (**a**), temperature (**b**), relative humidity (**c**), vapor pressure deficit (VPD) (**d**), wind speed (**e**), reference crop evapotranspiration (ET_o) (**f**) and sap flow (**g**). Arrows in (**a**) indicate the starting time of the top vent opening in winter season and solid lines indicate the duration of vent opening in spring and summer seasons. In autumn–winter season, the top vent was mostly opened from 9:00 to 11:00 on sunny days and was opened all day in spring and summer seasons. Typical days shown in Figure 3: 29–30 December in 2018 (2018AW), 21–22 May in 2019 (2019SP), 30–31 July in 2019 (2019SU) and 19–20 December in 2019 (2019AW).

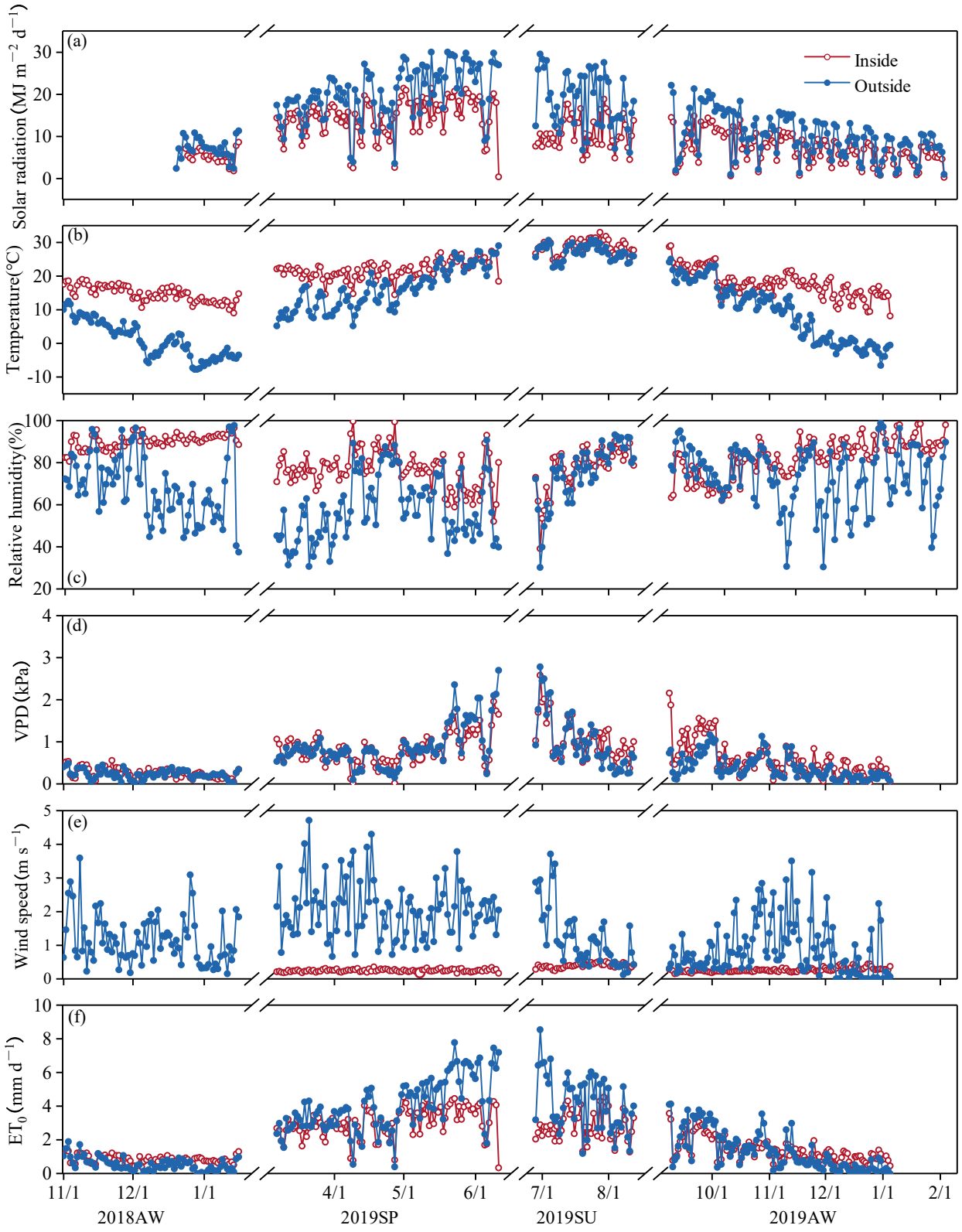

Figure 4. Seasonal variations of daily total solar radiation (**a**), mean temperature (**b**), relative humidity (**c**), vapor pressure deficit (VPD) (**d**), wind speed (**e**) and reference crop evapotranspiration (ET_o) (**f**).

Table 3. Linear regression parameters for the relationships between inside and outside solar radiation, air temperature, relative humidity, VPD, wind speed and ET_o in the four planting seasons. Inside and outside factors are dependent and independent variables in the regressed lines, respectively. Term "R^2" is the coefficient of determination for the corresponding regressed line.

Microclimate Variables	Experimental Seasons	Regressed Lines	R^2
Solar radiation ($MJ\ m^{-2}\ d^{-1}$)	2018AW	Ra(in) = 0.72Ra(out)	0.97 **
	2019SP	Ra(in) = 0.72Ra(out)	0.96 **
	2019SU	Ra(in) = 0.68Ra(out)	0.98 **
	2019AW	Ra(in) = 0.70Ra(out)	0.99 **
Temperature (°C)	2018AW	T(in) = 0.33T(out) + 14.34	0.60 **
	2019SP	T(in) = 0.34T(out) + 16.46	0.60 **
	2019SU	T(in) = 0.82T(out) + 6.55	0.78 **
	2019AW	T(in) = 0.37T(out) + 14.45	0.65 **
Relative humidity (%)	2018AW	RH(in) = 0.05RH(out) + 86.49	0.06 *
	2019SP	RH(in) = 0.39RH(out) + 54.01	0.45 **
	2019SU	RH(in) = 0.71RH(out) + 24.07	0.93 **
	2019AW	RH(in) = 0.20RH(out) + 67.82	0.10 **
VPD (kPa)	2018AW	VPD(in) = 0.80VPD(out) + 0.07	0.51 **
	2019SP	VPD(in) = 0.64VPD(out) + 0.26	0.77 **
	2019SU	VPD(in) = 0.69VPD(out) + 0.39	0.88 **
	2019AW	VPD(in) = 1.21VPD(out) + 0.11	0.66 **
Wind speed ($m\ s^{-1}$)	2018AW	/	/
	2019SP	Wind(in) = −0.009Wind(out) + 0.26	0.04
	2019SU	Wind(in) = −0.037Wind(out) + 0.43	0.24 **
	2019AW	Wind(in) = −0.010Wind(out) + 0.27	0.02
Daily ET_o ($mm\ d^{-1}$)	2018AW	ET_o (in) = 0.42 ET_o (out) + 0.60	0.45 **
	2019SP	ET_o (in) = 0.48 ET_o (out) + 1.16	0.78 **
	2019SU	ET_o (in) = 0.71 ET_o (out) + 0.25	0.95 **
	2019AW	ET_o (in) = 0.57 ET_o (out) + 0.64	0.88 **

Note: "*" and "**" after numbers in the column "R^2" indicates the regression lines are significant at 0.05 and 0.01 level, respectively.

Inside solar radiation was linearly related to that outside in the four experimental seasons (R^2 of 0.96–0.99). Slopes of the regression lines, i.e., the seasonal mean transmission, ranged from 0.68 to 0.72. Inside air temperatures were much higher than outside during winter. In December 2018, the inside daily maximum, minimum and mean temperatures exceeded those outside by 22.6, 16.7 and 15.8 °C, respectively, and 21.3, 17.9 and 16.3 °C in January. Similarly, in December 2019, inside daily maximum, minimum and mean temperatures exceeded those outside by 22.9, 15.2 and 15.1 °C. On 30 December 2019, temperatures exceeded those outside by 36.9, 22.0 and 19.8 °C (corresponding to outdoor 1.0, −13.1 and −2.9 °C). Inside temperatures were close to outside from April to October, due to the strong exchanges of heat and mass when the top and side vents were fully opened during this period.

In the winter periods of 2018AW and 2019AW, seasonal mean inside RH values were 90.2% and 88.4%, respectively, higher than that (68.1% and 72.0%) outside. However, in summer inside humidity (77.4%) was close to that (75.3%) outside because top and side vents were open all day. Seasonal mean VPDs inside were 0.82 and 1.07 kPa in 2019SP and 2019SU, which were close to those (0.88 and 0.98 kPa) outside. In the winter periods of 2018AW and 2019AW, daily mean VPDs were 0.29 and 0.35 kPa, respectively, and correspondingly higher than those (0.21 and 0.24 kPa) outside. This high inside VPD is mainly because of the higher inside temperature. Inside VPD was less related to that outside in winter (R^2 = 0.51 in 2018AW season, and 0.66 in 2019AW season), which could be due to isolated inside environmental conditions caused by the short ventilation period (1–2 h on sunny days or closed all the time on cloudy and snowy days).

Inside daily mean air velocity ranged from 0.14 m s^{-1} to 0.53 m s^{-1} with seasonal means of 0.24 m s^{-1}, 0.39 m s^{-1} and 0.26 m s^{-1}, in 2019SP, 2019SU and 2019AW, respectively. However, outside wind speed varied from 0.1 m s^{-1} to 4.71 m s^{-1} in the same period. The lower air velocity with slight variation inside the greenhouse compared to that outside indicates that inside air velocity is less affected by that outside because of the greenhouse cover.

Generally, outside daily ET_o was higher than that inside in spring and summer. However, in winter the inside daily ET_o was slightly higher than that outside, especially in the period from mid-November to mid-January in both the 2018AW and 2019AW seasons. This is due to the increased inside VPD (+0.02~0.11 kPa or 10~46%) caused by higher temperature (+13.3~13.7 °C) compared to that outside. Total inside ET_o values in the SF measurement period in the 2018AW, 2019SP, 2019SU and 2019AW seasons were 64, 184, 101 and 74 mm, respectively, compared to 41, 264, 136 and 51 mm outside. Thus, inside ET_o was about 1.51 times that outside in winter, and 0.71 on average in spring and summer.

The daily course of SF (Figure 3g) was similar to that of ET_o, and both were high in spring and summer and low in autumn and winter. ET_o started at 6:00 then increased to a peak value at 12:00 and thereafter gradually decreased to zero after 18:00 in the 2019SP and 2019SU planting seasons. Similarly, SF reached its peak value during 11:00–13:00 in the autumn–winter planting season. Sap flow was observed from 9:00 to 16:00 in the winter season. This period is much shorter than that in spring and summer seasons (from 6:00 to 18:00), because of the shorter day length and early mat covering before sunset in the winter. The large changes in SF at different periods is in agreement with the yearly curve of ET_o (Figure 4f), indicating strong coupling between plant transpiration and microclimate.

Inside daily mean soil temperatures at 10, 20, 30 and 40 cm depths in the four seasons are shown in Figure 5. Differences in soil temperatures at the four depths were small. However, these soil temperatures show clear seasonal and annual changes. Monthly mean soil temperature at 10 cm depth was the lowest, approximately 12 °C, in January, and increased to approximately 30 °C in August. Generally, the seasonal mean soil temperature at 10 cm depth was 12–25 °C in autumn–winter, 20–25 °C in spring and 25–30 °C in summer.

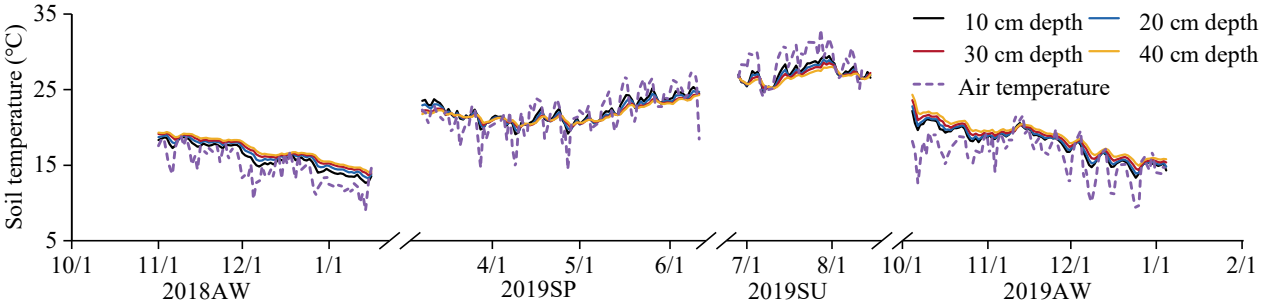

Figure 5. Changes of inside daily mean soil temperatures at 10, 20, 30 and 40 cm depth and inside air temperature in the four seasons.

4.3. Daily Total Sap Flow and Basal Crop Coefficient

Daily total SF in different seasons had different trends (Figure 6). Generally, SF was higher in spring and summer (2019SP and 2019SU seasons) and lower in autumn and winter (2018AW and 2019AW). In spring, SF reached the highest value of approximately 5 mm day^{-1}, while the maximum SF was only 3.6 mm day^{-1} in autumn–winter. Most daily SF in the spring and summer varied between 2 and 4 mm day^{-1}. However, in autumn and winter (2018AW and 2019AW seasons), most SF ranged from 1 to 3 mm day^{-1}.

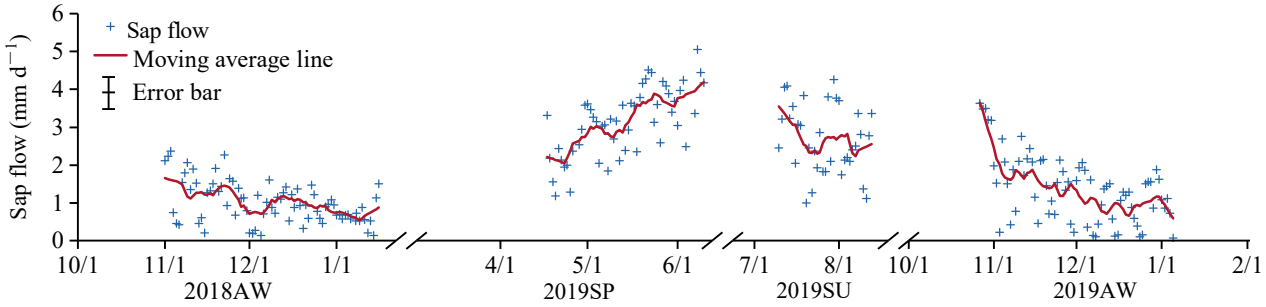

Figure 6. Seasonal course of sap flow. The red line is the 5-day moving average. The average error over the four seasons is ±0.3 mm d^{-1}.

SF was measured during fruit expansion and ripening when the plant stem was strong enough to hold the sensors and total leaf area changed slightly. The basal crop coefficient K_{cb}, i.e., the ratio of SF to ET_o, was calculated and results are shown in Figure 7. The trend of K_{cb} was much smoother than that for SF (Figure 6). Values and pattern in the autumn–winter period of 2018AW and 2019AW were similar, with mean K_{cb} of 1.1 and 1.2, respectively. During the later period, 2018AW, K_{cb} decreased from 1.2 to 0.8 because of leaf aging and the decrease of LAI from 2.9 to 2.2. The K_{cb} patterns in spring and summer of 2019SP and 2019SU were similar. The mean value of 0.90 in both seasons was lower than those in the winter periods and varied slightly.

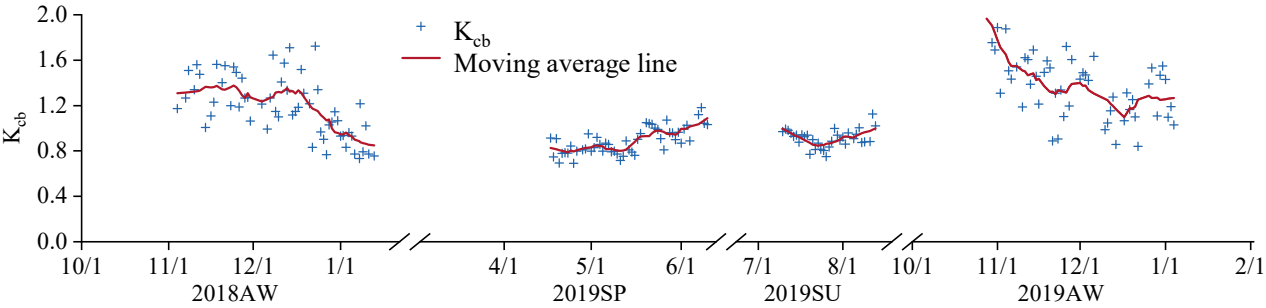

Figure 7. Seasonal course of K_{cb}. The red line is the 5-day moving average.

4.4. Crop Growth Factors and Fresh Tomato Yield

Plant growth indexes (including plant height and leaf area index) of tomato in the four planting seasons are shown in Table 4. Plant height and leaf area were measured from the time when plant height reached about 100 cm. After that, leaf area was high and water consumption increased sharply.

In the SF measurement period, maximum plant height reached 170 cm, and leaf area index (LAI) was between 0.92 and 3.35. Due to the artificial pruning performed in the middle of tomato growing, plant height and LAI increased at first, but were later maintained constant in the latter growth period. The 2019SU planting season was different, when, as noted, growth was very poor due to the high inside temperature and the crop was aborted prematurely.

Tomato yield was the largest with 138.0 ton ha^{-1} in the 2019 SP season, followed by 86.5 ton ha^{-1} in the 2018AW season and 56.3 ton ha^{-1} in the 2019 AW season. These yields were close to reported yields of 60–140 ton ha^{-1} per season in greenhouses in the North China Plain and Northwest China [34,55,56]. Tomato yield in the 2019SU season (10.8 ton ha^{-1}) was much lower than that (56–138 ton ha^{-1}) in the other three seasons due to the extremely high inside temperatures (mean daily maximum temperature of 38.1 °C), which destroyed plant growth and finally resulted in much lower yield [57,58]. This indicates that this SSG is not suitable for tomato cultivation in summer in North China.

Table 4. LAI, plant height and yield in each tomato growth season.

Planting Seasons	Date	LAI	Plant Height/cm	Seasonal Yield/ton ha^{-1}
2018AW	1 November 2018	2.86	165	86.5
	1 January 2019	2.20	147	
2019SP	23 March 2019	2.23	148	138.0
	13 April 2019	3.35	154	
	28 April 2019	3.09	159	
	5 May 2019	1.92	170	
	19 May 2019	1.80	133	
	7 June 2019	2.26	149	
2019SU	27 June 2019	1.41	102	10.8
	15 July 2019	2.07	142	
	26 July 2019	2.19	150	
	6 August 2019	2.27	160	
	16 August 2019	2.34	170	
2019AW	4 October 2019	0.92	81	56.3
	26 October 2019	1.62	119	
	23 November 2019	1.55	125	
	21 December 2019	1.68	123	

5. Discussion

5.1. Sap Flow and Microclimate Variables

Under ample soil water, sap flow is mainly governed by climate and plant morphology, such as LAI [19,59]. We found that the shapes of the daily curves of sap flow followed those of the inside microclimate (Figure 3). This indicates that SF is strongly coupled to inside solar radiation, air temperature and VPD. Similar findings were reported for tomato and rose plants in greenhouse cultivation [14,19,26] as well as in forest stands [27,60,61].

Figure 8 shows the relationships between daily SF and total radiation VPD and daily average temperature, respectively. The highest R^2 of 0.85–0.97 was found in the linear regression between daily SF and solar radiation, explaining more than 85% of the variation of SF. This implies that the total radiation may be used to predict the daily sap flow of tomato inside this SSG. The slope ranged from 0.19 to 0.24 in the 2019SP, 2019SU and 2019AW seasons, while it was 0.15 in the 2018AW season. When all data were pooled the slope was 0.20. Strong linear correlations between tomato sap flow and radiation in greenhouses have been reported previously [26,27]. Li et al. [62] modeled tomato plant transpiration in a greenhouse using the random forest regression algorithm and found that radiation intensity had the greatest effect on plant transpiration.

Daily SF was linearly correlated to VPD, as shown in Figure 8b. The high R^2 values of 0.85 and 0.91 between SF and VPD were for the autumn–winter season. The slope of the linear regression line was 4.13 mm d^{-1} kPa^{-1} in 2018AW and close to that (3.61 mm d^{-1} kPa^{-1}) in 2019AW, indicating that the relationship is consistent in the winter period. The R^2 for these regressions ranged from 0.58 to 0.91, which is lower than that for solar radiation (0.85–0.97; Figure 8a). This is consistent with other studies [28,63]. However, Feng et al. [64] found in a greenhouse that the correlation between the transpiration of pear–jujube trees and VPD was better than that with radiation. This may be due to the deficit irrigation and resulting water stress in their experiment. Plant transpiration under water deficit is dominated by soil water availability and less by radiation, and then plants adjust transpiration according to VPD. Thus, for the well-watered crop in this study, daily SF in the winter could be estimated from the VPD relationship, while in spring and summer other factors should be taken into account to estimate SF along with VPD.

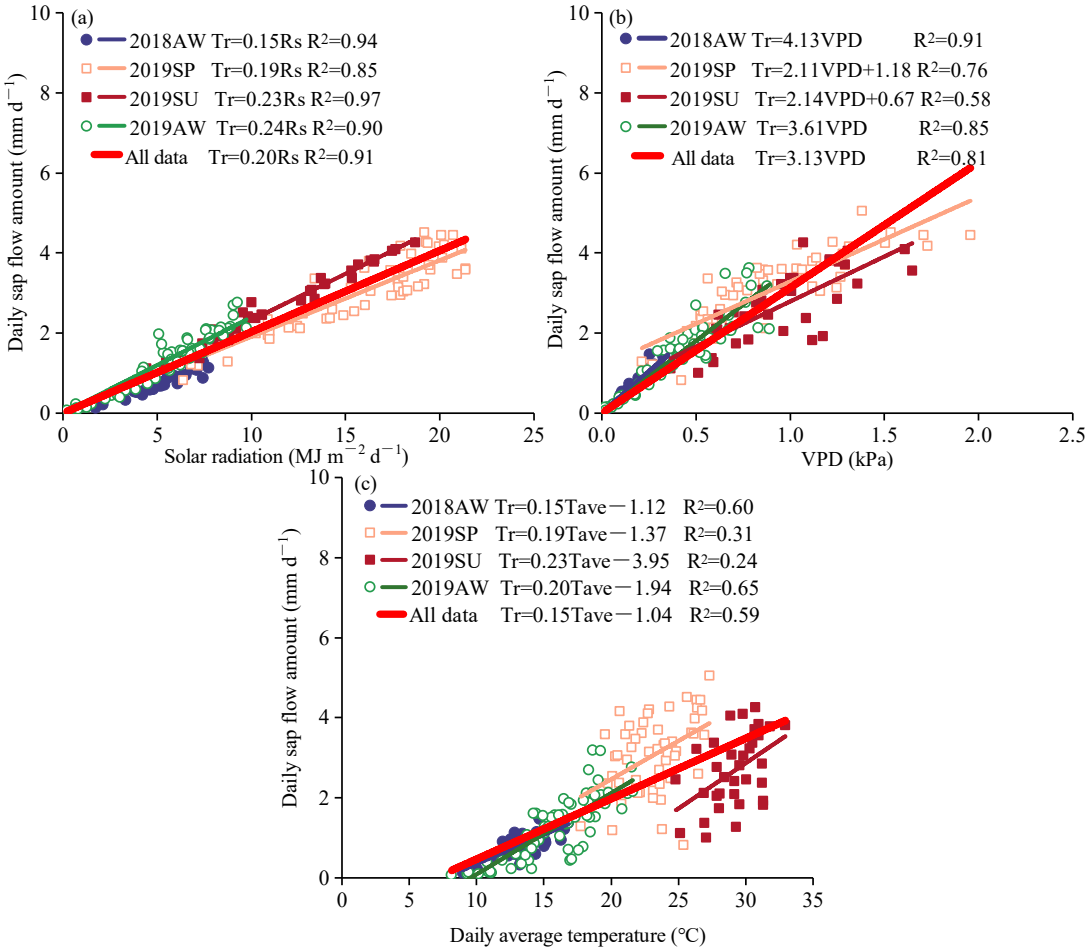

Figure 8. Linear regression results of daily sap flow and solar radiation (**a**), VPD (**b**) and daily average temperature (**c**). Daily sap flow and microclimate variables are dependent and independent variables in the regressed lines, respectively.

The relationships between SF and temperature can also be fitted with linear equations, but the R^2 values of 0.60–0.65 in the winter and 0.24–0.31 in spring and summer were much lower than those for radiation and VPD. This indicates that estimating sap flow using temperature could introduce large errors compared to radiation and VPD. Similar results were reported elsewhere [65,66].

Over the four seasons, daily SF was more closely related to radiation, VPD and temperature in the autumn and winter period than in spring and summer. This is probably due to the isolated microclimate in autumn and winter due to the short time of ventilation. In the spring and autumn, the vent was opened all day, which enhanced energy and mass exchanges between inside and outside. Thus, when ventilation is for a longer time, plant transpiration is affected by multi-microclimate variables and its estimation may require more microclimate variables.

5.2. Basal Crop Coefficient Variation

During the middle growth stage, plants generally reach the highest LAI when all leaves are fully grown, and plants have the highest evapotranspiration when soil water is sufficient [67,68]. The dominating factors for crop ET_a in this period were climatic and can be integrated using ET_o. The basal crop coefficient K_{cb}, the ratio of crop transpiration to ET_o, in this stage varies slightly and is taken as a constant (Allen et al., 1998). In this study, the sap flow was measured during the fruit expansion and ripening period, when the plant is at maximum LAI (Table 4).

During the middle stage when the SF was measured, there is a significant linear correlation between SF and ET_o in the four seasons inside the SSG (Figure 9). The R^2 in the regression line between SF and ET_o was the highest in the 2019SU season (0.95), followed by that in the 2019SP season (0.83). Lower R^2 values of 0.66 and 0.76 were found in the 2018AW and 2019AW seasons, respectively. In the 2019SU season, LAI ranged from 2.07 to 2.34 during the SF measurement period (Table 4), which provided a relatively uniform transpiration surface and resulted in an excellent linear relationship between SF and ET_o. However, in the other three seasons, LAI had more variation because of top cutting and leaf trimming, which induced large variation in SF and more deviation from the regression line.

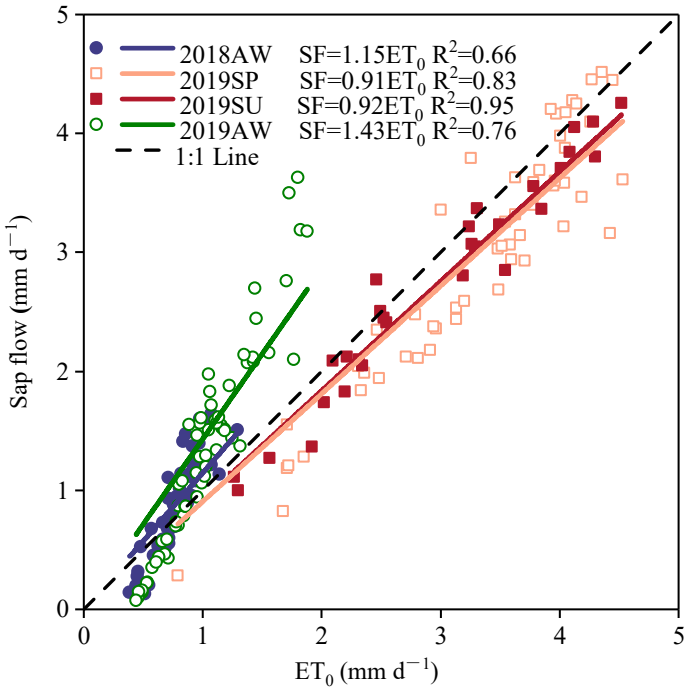

Figure 9. Linear regressions of inside daily sap flow and ET_o in the four experimental seasons.

The relationship between SF and ET_o was similar in the two winter seasons (2018AW and 2019AW) and that in spring (2019SP season) was similar to summer (2019SU season) (Figure 9). However, the relationship in winter was significantly different from that in spring and summer. If the intercepts of the regression lines are taken as zero, the slopes, i.e., K_{cb}, were 1.15 and 1.43 in 2018AW and 2019AW, respectively, and 0.91 and 0.92 in spring and summer, respectively. In a solar greenhouse in North China, in the middle and late stage of the tomato growth period, K_{cb} ranged from 1.02 to 0.65 in spring and summer (from March to July), and basal crop coefficients in the middle stage were 0.94–1.02 [69], which are close to the values reported here. Thus, based on the linear regression results in Figure 9, the crop's SF in the winter period could be 30–60% higher than in spring and summer for the same ET_o. Even so, the actual SF in the fruit growth stages in spring and summer was on average about 16% higher than that in the winter period because of the higher ET_o (Figure 3f,g). These results highlight that plant resistance increases with VPD, which in this case resulted in moderate stabilization of SF.

The FAO recommendation for K_{cb} in the middle stage for tomato is 1.15 when crop height is 1.5–2.0 m high [48]. That K_{cb} value is slightly smaller than those found here in the winter season (1.15–1.43), and higher than those in spring and summer (0.91–0.92) reported here. Orgaz et al. [69] investigated crop coefficients of four crops in an unheated plastic greenhouse in the Mediterranean and found that peak K_c values for vertically supported greenhouse crops (melon, green beans, watermelon and pepper) varied between 1.3 and 1.4, which are higher than those reported for outdoors. They explained that the tall and open canopy structures of the vertical supported greenhouse crops, along with

the high proportion of diffuse radiation inside the greenhouse, allowed for more uniform light penetration into the canopies and enhanced transfer of heat and water vapor [70]. That resulted in higher crop ET rates and finally higher crop coefficients than those of short, non-supported crops. However, Qiu et al. [71] found that in the early and middle growth stages of greenhouse tomatoes with different planting density, the crop coefficient in autumn and winter was between 0.77 and 0.83 in the first season and between 0.94 and 0.97 in the second season, which are smaller than those reported here. Thus, we conclude that crop coefficients may vary with greenhouse and plantation density. Therefore, when calculating crop ET_a and planning irrigation in the greenhouse, tomato growth stage, season, greenhouse structure and planting density should be considered.

5.3. Decoupling Coefficient (Ω)

The decoupling coefficient (Ω) is an important parameter to characterize the water vapor exchange between crops and the surrounding atmosphere, which can reflect the degree of stomatal control on transpiration. It was calculated by using measured stomatal conductance, plant morphology (LAI and plant height) and meteorological data, using Equation (3). The daily courses of Ω and the corresponding air velocity and leaf conductance are shown in Figure 10.

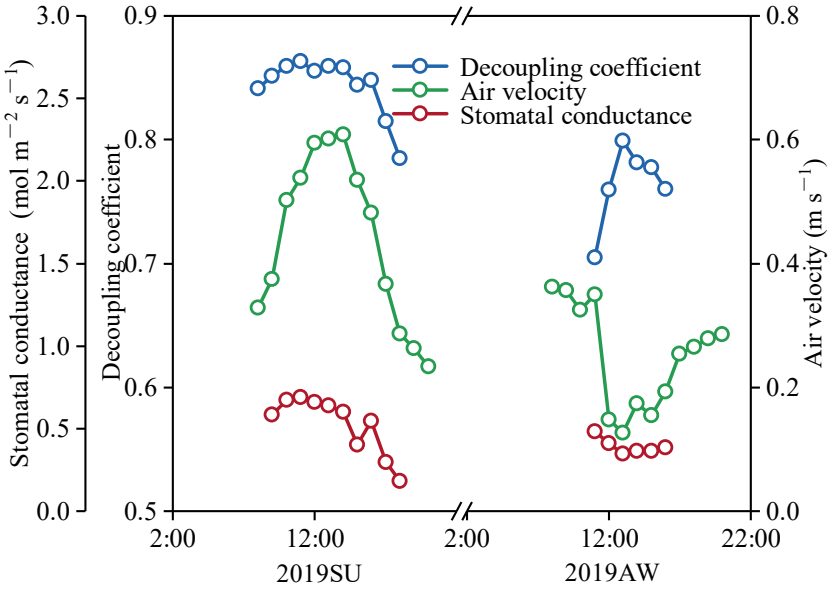

Figure 10. Average daily courses (15 July 2019 and 21 December 2019) of the air velocity, stomatal conductance and decoupling coefficient.

The decoupling coefficient before 16:00 in summer was about 0.85 and varied slightly, after that it decreased due to the decline of g_s from 0.6 to 0.2 mol m^{-2} s^{-1} [72]. In other words, canopy resistance, r_c, increased from 65 s m^{-1} before 16:00 to 165 s m^{-1} at 18:00, and that led to a decrease in Ω as air velocity decreased. In winter the decoupling coefficient increased from 0.70 at 11:00 to 0.80 at 13:00, then slightly decreased. The higher air velocity in the morning could be the main reason for lower Ω. The average value of the decoupling coefficient in daytime in summer (0.84) was higher than that in winter (0.76). However, these two Ω values are much higher than those for crops and forest plantations in open fields (generally <0.5) [72], indicating that inside transpiration is mainly controlled by net radiation and less by stomata. Transpiration in both winter and summer is largely decoupled from the aerodynamic environment, as confirmed in Figure 8, which shows the close relationship between transpiration and radiation. The stronger relationship between transpiration and VPD in winter (Figure 8) agrees with the finding that Ω in winter is slightly smaller than that in summer.

5.4. Irrigation Efficiency and Irrigation Scheduling

Irrigation efficiency is defined as the ratio of crop evapotranspiration to irrigation water applied [52,73]. This index can be used to evaluate irrigation systems, irrigation scheduling and irrigation management. In the first season (2018AW), the farmer irrigated based on his personal experience. The total irrigation amount of 255 mm was much higher than the 78 mm of plant transpiration during the SF measurement period, resulting in the lowest IE, 0.31. This indicates approximately 70% irrigation water is lost.

In the following three seasons, a tensiometer, installed at 20 cm depth in the root zone, was used for irrigation timing. With the tensiometer, the farmer started irrigation at −25~−35 kPa and we recommended an irrigation depth of 10 mm for each irrigation. With this irrigation scheduling, soil water content declined into the optimal region [53]. In fact, the measured soil matric potentials (SMP) at 20 cm depth in the 2018AW and 2019AW seasons were generally higher than −30 kPa, and reached −50 kPa a few times before irrigation in the 2019SP and 2019SU seasons. The actual irrigation depth per event ranged from 15.5 mm in the 2019SU season to 33.1 mm in the 2019SP season, which was still much lower than the 42.5 mm in the 2018AW season. Although irrigation depth was higher than we recommended, irrigation was still reduced by more than half in the last seasons. In the 2019SP and 2019AW seasons, the measured SFs were 165 mm and 98 mm, respectively, and the corresponding irrigation depths were 265 and 162 mm, which resulted in IEs of 0.62 and 0.60, respectively. It was found that the increased IE of 0.60–0.62 in the 2019SP and 2019AW seasons were much higher than that of 0.31 in the first season. We conclude that although IE increased by >100% in the 2019SP and 2019AW seasons using the recommended method, there is room for further improvement. In the 2019SU planting season, IE reached 3.07 due to the poor growth of crops in the later stage, and farmers reduced irrigation in order to reduce costs.

Optimal irrigation scheduling includes irrigation timing and amount. Our study shows that tomato crop transpiration varied slightly when SMP was higher than −35 kPa in winter, spring and summer seasons, in agreement with other studies [74–76]. Therefore, an SMP threshold of −35 kPa is recommended for greenhouse cultivation in the study region.

6. Conclusions

In this study, a four-season experiment was carried out in a newly developed sunken solar greenhouse in the NCP. Inside microclimate, tomato transpiration rate and crop coefficients were analyzed and compared in these four seasons. We conclude that:

(1) All micrometeorological variables were linearly related to those outside, except for wind speed in all seasons, indicating that most meteorological factors were strongly coupled to outside.
(2) Daily sap flow of tomato crops was best related to solar radiation, followed by VPD and temperature. The close relationship between sap flow and radiation indicates that crop transpiration is decoupled from the aerodynamic environment, as confirmed by the high decoupling coefficients, 0.84 in summer and 0.76 in winter.
(3) The basal crop coefficient at the middle stage was 1.15–1.43 in autumn and winter, and 0.91–0.92 in spring and summer, indicating high evapotranspiration potential in winter for the same ET_o.
(4) An optimized irrigation scheduling is recommended for tomato in this SSG, in which crop coefficients can refer to those found here and a threshold soil water matric potential for irrigation is −35 kPa.

Author Contributions: Conception and design of experiments: H.L.; performance of experiments and analysis of data: L.Y. and Z.G.; writing—review and editing: L.Y., H.L. and S.C. All authors have read and agreed to the published version of the manuscript.

Funding: This work was supported by the Science and Technology Major Project of Inner Mongolia Autonomous (NO. NMKJXM202105), National Nature Science Foundation of China (NO. 91479004, 51939005) and the 111 Project (B18006).

Institutional Review Board Statement: Not applicable.

Informed Consent Statement: Not applicable.

Acknowledgments: We greatly appreciate the cooperation of Jiaqi Wang, the owner of the solar greenhouse.

Conflicts of Interest: The authors declare no conflict of interest.

References

1. Incrocci, L.; Thompson, R.B.; Fernandez-Fernandez, M.D.; De Pascale, S.; Pardossi, A.; Stanghellini, C.; Rouphael, Y.; Gallardo, M. Irrigation management of European greenhouse vegetable crops. *Agric. Water Manag.* **2020**, *242*, 106393. [CrossRef]
2. Rouphael, Y.; Kyriacou, M.C.; Petropoulos, S.A.; De Pascale, S.; Colla, G. Improving vegetable quality in controlled environments. *Sci. Hortic.* **2018**, *234*, 275–289. [CrossRef]
3. Yuan, B.-Z.; Sun, J.; Kang, Y.; Nishiyama, S. Response of cucumber to drip irrigation water under a rainshelter. *Agric. Water Manag.* **2006**, *81*, 145–158. [CrossRef]
4. Zhang, X. Progress of mechanised agriculture in China. *Agric. Mech. Inform.* **2020**, *2020*, 1–16.
5. Chen, S.N.; Li, Z.F.; Liu, F.; Yang, S.B.; Li, M. Risk evaluation of solar greenhouse cucumbers low temperature disaster based on GIS spatial analysis in Tianjin, China. *Geomat. Nat. Hazards Risk* **2019**, *10*, 576–598. [CrossRef]
6. Gong, X.; Liu, H.; Sun, J.; Gao, Y.; Zhang, H. Comparison of Shuttleworth-Wallace model and dual crop coefficient method for estimating evapotranspiration of tomato cultivated in a solar greenhouse. *Agric. Water Manag.* **2019**, *217*, 141–153. [CrossRef]
7. Cao, K.; Xu, H.J.; Zhang, R.; Xu, D.W.; Yan, L.L.; Sun, Y.C.; Xia, L.R.; Zhao, J.T.; Zou, Z.R.; Bao, E.C. Renewable and sustainable strategies for improving the thermal environment of Chinese solar greenhouses. *Energy Build.* **2019**, *202*, 109414. [CrossRef]
8. Xu, F.; Li, S.; Ma, C.; Zhao, S.; Han, J.; Liu, Y.; Hu, B.; Wang, S. Thermal Environment of Chinese Solar Greenhouses: Analysis and Simulation. *Appl. Eng. Agric.* **2013**, *29*, 991–997.
9. Singh, M.C.; Singh, J.P.; Singh, K.G. Development of a microclimate model for prediction of temperatures inside a naturally ventilated greenhouse under cucumber crop in soilless media. *Comput. Electron. Agric.* **2018**, *154*, 227–238. [CrossRef]
10. Tang, Y.L.; Ma, X.; Li, M.; Wang, Y.F. The effect of temperature and light on strawberry production in a solar greenhouse. *Sol. Energy* **2020**, *195*, 318–328. [CrossRef]
11. Baddadi, S.; Bouadila, S.; Guizani, A. Beneficial use of two packed beds of latent storage energy for the heating of a hydroponic greenhouse. *Energy Procedia* **2019**, *162*, 156–163. [CrossRef]
12. Gourdo, L.; Fatnassi, H.; Bouharroud, R.; Ezzaeri, K.; Bazgaou, A.; Wifaya, A.; Demrati, H.; Bekkaoui, A.; Aharoune, A.; Poncet, C.; et al. Heating canarian greenhouse with a passive solar water–sleeve system: Effect on microclimate and tomato crop yield. *Sol. Energy* **2019**, *188*, 1349–1359. [CrossRef]
13. Hassanain, A.A.; Hokam, E.M.; Mallick, T.K. Effect of solar storage wall on the passive solar heating constructions. *Energy Build.* **2011**, *43*, 737–747. [CrossRef]
14. Li, B.; Shi, B.J.; Yao, Z.Z.; Shukla, M.K.; Du, T.S. Energy partitioning and microclimate of solar greenhouse under drip and furrow irrigation systems. *Agric. Water Manag.* **2020**, *234*, 106096. [CrossRef]
15. Shukla, A.; Sharma, A.; Kant, K. Solar Greenhouse with Thermal Energy Storage: A Review. *Curr. Sustain. Renew. Energy Rep.* **2016**, *3*, 58–66. [CrossRef]
16. Tong, G.H.; Christopher, D.M.; Li, T.L.; Wang, T.L. Passive solar energy utilization: A review of cross-section building parameter selection for Chinese solar greenhouses. *Renew. Sust. Energy Rev.* **2013**, *26*, 540–548. [CrossRef]
17. Ren, J.; Zhao, Z.; Zhang, J.; Wang, J.; Guo, S.R.; Sun, J. Study on the hygrothermal properties of a Chinese solar greenhouse with a straw block north wall. *Energy Build.* **2019**, *193*, 127–138. [CrossRef]
18. Saberian, A.; Sajadiye, S.M. The effect of dynamic solar heat load on the greenhouse microclimate using CFD simulation. *Renew. Energy* **2019**, *138*, 722–737. [CrossRef]
19. Liu, F.; Cohen, Y.; Fuchs, M.; Plaut, Z.; Grava, A. The effect of vapor pressure deficit on leaf area and water transport in flower stems of soil-less culture rose. *Agric. Water Manag.* **2006**, *81*, 216–224. [CrossRef]
20. Linker, R.; Kacira, M.; Arbel, A. Robust climate control of a greenhouse equipped with variable-speed fans and a variable-pressure fogging system. *Biosyst. Eng.* **2011**, *110*, 153–167. [CrossRef]
21. Ahemd, H.A.; Al-Faraj, A.A.; Abdel-Ghany, A.M. Shading greenhouses to improve the microclimate, energy and water saving in hot regions: A review. *Sci. Hortic.* **2016**, *201*, 36–45. [CrossRef]
22. Li, A.G.; Huang, L.; Zhang, T.F. Field test and analysis of microclimate in naturally ventilated single-sloped greenhouses. *Energy Build.* **2017**, *138*, 479–489. [CrossRef]
23. Liu, H.J.; Cohen, S.; Lemcoff, J.H.; Israeli, Y.; Tanny, J. Sap flow, canopy conductance and microclimate in a banana screenhouse. *Agric. For. Meteorol.* **2015**, *201*, 165–175.
24. Sangpradit, K. Study of the solar transmissivity of plastic cladding materials and influence of dust and dirt on greenhouse cultivations. *Energy Procedia* **2014**, *56*, 566–573. [CrossRef]

25. Ni, M.; Lan, D.; Jahan, M.S.; Wang, J.; Guo, S. A Pilot Study on the Microclimate of a Multi-Span Solar Energy Greenhouse. *Appl. Eng. Agric.* **2019**, *35*, 601–616. [CrossRef]
26. Gong, X.W.; Qiu, R.J.; Sun, J.S.; Ge, J.K.; Li, Y.B.; Wang, S.S. Evapotranspiration and crop coefficient of tomato grown in a solar greenhouse under full and deficit irrigation. *Agric. Water Manag.* **2020**, *235*, 106154. [CrossRef]
27. Mao, H.P.; Ullah, I.; Ni, J.H.; Javed, Q.; Azeem, A. Estimating tomato water consumption by sap flow measurement in response to water stress under greenhouse conditions. *J. Plant Interact.* **2017**, *12*, 402–413.
28. Olufayo, A.A.; Oguntunde, P.G.; Omotayo, F.S. Influence of Climatic Variables on Whole-plant Water use of Cocoa under Limited Soil Moisture Condition. *J. Agric. Ecol. Res. Int.* **2019**, *19*, 1–8.
29. Wu, Y.S.; Gong, W.Z.; Wang, Y.M.; Yang, W.Y. Shading of mature leaves systemically regulates photosynthesis and leaf area of new developing leaves via hormones. *Photosynthetica* **2019**, *57*, 303–310. [CrossRef]
30. Chen, D.Y.; Wang, Y.K.; Liu, S.Y.; Wei, X.G.; Wang, X. Response of relative sap flow to meteorological factors under different soil moisture conditions in rainfed jujube (*Ziziphus jujuba* Mill.) plantations in semiarid Northwest China. *Agric. Water Manag.* **2014**, *136*, 23–33. [CrossRef]
31. Brito, P.; Lorenzo, J.R.; Gonzalez-Rodriguez, A.M.; Morales, D.; Wieser, G.; Jimenez, M.S. Canopy transpiration of a semi arid Pinus canariensis forest at a treeline ecotone in two hydrologically contrasting years. *Agric. For. Meteorol.* **2015**, *201*, 120–127. [CrossRef]
32. Clausnitzer, F.; Köstner, B.; Schwärzel, K.; Bernhofer, C. Relationships between canopy transpiration, atmospheric conditions and soil water availability—Analyses of long-term sap-flow measurements in an old Norway spruce forest at the Ore Mountains/Germany. *Agric. For. Meteorol.* **2011**, *151*, 1023–1034. [CrossRef]
33. Yang, Z.Q.; Xu, C.; Wang, M.T.; Zhao, H.L.; Zheng, Y.J.; Huang, H.J.; Vuguziga, F.; Umutoni, M.A. Enhancing the thermotolerance of tomato seedlings by heat shock treatment. *Photosynthetica* **2019**, *57*, 1184–1192. [CrossRef]
34. He, F.F.; Chen, Q.; Jiang, R.F.; Chen, X.P.; Zhang, F.S. Yield and nitrogen balance of greenhouse tomato (*Lycopersicum esculentum* Mill.) with conventional and site-specific nitrogen management in northern China. *Nutr. Cycl. Agroecosyst.* **2007**, *77*, 1–14. [CrossRef]
35. Zhou, H.P.; Kang, S.Z.; Li, F.S.; Du, T.S.; Shukla, M.K.; Li, X.J. Nitrogen application modified the effect of deficit irrigation on tomato transpiration, and water use efficiency in different growth stages. *Sci. Hortic.* **2020**, *263*, 109112. [CrossRef]
36. Lv, H.; Lin, S.; Wang, Y.; Lian, X.; Zhao, Y.; Li, Y.; Du, J.; Wang, Z.; Wang, J.; Butterbach-Bahl, K. Drip fertigation significantly reduces nitrogen leaching in solar greenhouse vegetable production system. *Environ. Pollut.* **2019**, *245*, 694–701. [CrossRef]
37. Sun, Y.; Hu, K.L.; Fan, Z.B.; Wei, Y.P.; Lin, S.; Wang, J.G. Simulating the fate of nitrogen and optimizing water and nitrogen management of greenhouse tomato in North China using the EU-Rotate_N model. *Agric. Water Manag.* **2013**, *128*, 72–84. [CrossRef]
38. National Bureau of Statistics of China. *China National Statistical Yearbook*; China Statistics Press: Beijing, China, 2019.
39. Hernandez-Espinoza, L.H.; Barrios-Masias, F.H. Physiological and anatomical changes in tomato roots in response to low water stress. *Sci. Hortic.* **2020**, *265*, 109208. [CrossRef]
40. Sato, S.; Peet, M.M.; Thomas, J.F. Physiological factors limit fruit set of tomato (*Lycopersicon esculentum* Mill.) under chronic, mild heat stress. *Plant Cell Environ.* **2000**, *23*, 719–726. [CrossRef]
41. Firon, N.; Shaked, R.; Peet, M.M.; Pharr, D.M.; Zamski, E.; Rosenfeld, K.; Althan, L.; Pressman, E. Pollen grains of heat tolerant tomato cultivars retain higher carbohydrate concentration under heat stress conditions. *Sci. Hortic.* **2006**, *109*, 212–217. [CrossRef]
42. De Swaef, T.; Verbist, K.; Cornelis, W.; Steppe, K. Tomato sap flow, stem and fruit growth in relation to water availability in rockwool growing medium. *Plant Soil* **2011**, *350*, 237–252. [CrossRef]
43. Ghorbanpour, A.; Salimi, A.; Ghanbary MA, T.; Pirdashti, H.; Dehestani, A. The effect of Trichoderma harzianum in mitigating low temperature stress in tomato (*Solanum lycopersicum* L.) plants. *Sci. Hortic.* **2018**, *230*, 134–141. [CrossRef]
44. Hillel, D. *Introduction to Environmental Soil Physics*; Elsevier Academic Press: Amsterdam, The Netherlands, 2003.
45. Feng, Z.; Kang, Y.; Wan, S.; Liu, S. Effect of Drip Fertigation on Potato Productivity with Basal Application of Loss Control Fertilizer in Sandy Soil. *Irrig. Drain.* **2018**, *67*, 210–221. [CrossRef]
46. Sun, J.; Kang, Y.; Wan, S.; Hu, W. Influence of drip irrigation level on salt leaching and vegetation growth during reclamation of coastal saline soil having an imbedded gravel–sand layer. *Ecol. Eng.* **2017**, *108*, 59–69. [CrossRef]
47. Liu, H.; Yin, C.; Gao, Z.; Hou, L. Evaluation of cucumber yield, economic benefit and water productivity under different soil matric potentials in solar greenhouses in North China. *Agric. Water Manag.* **2021**, *243*, 106442. [CrossRef]
48. Allen, R.G.; Pereira, L.S.; Raes, D.; Smith, M. *Crop Evapotranspiration: Guidelines for Computing Crop Water Requirements*; Food and Agriculture Organization of the United Nations: Rome, Italy, 1998.
49. Jarvis, P.G.; McNaughton, K.G. Stomatal Control of Transpiration: Scaling Up from Leaf to Region. *Adv. Ecol. Res.* **1986**, *15*, 1–49.
50. Möller, M.; Tanny, J.; Li, Y.; Cohen, S.T. Measuring and predicting evapotranspiration in an insect-proof screenhouse. *Agric. For. Meteorol.* **2004**, *127*, 35–51. [CrossRef]
51. Fuchs, M. Transpiration and foliage temperature in a greenhouse. In Proceeding of the International Workshop, Tel Aviv, Israel, 2–6 May 1993.
52. Perry, C. Efficient irrigation; Inefficient communication; Flawed recommendations. *Irrig. Drain.* **2007**, *56*, 367–378. [CrossRef]
53. Shock, C.C.; Wang, F.X. Soil Water Tension, a Powerful Measurement for Productivity and Stewardship. *Hortscience* **2011**, *46*, 178–185. [CrossRef]

54. Wang, D.; Kang, Y.H.; Wan, S.Q. Effect of soil matric potential on tomato yield and water use under drip irrigation condition. *Agric. Water Manag.* **2007**, *87*, 180–186. [CrossRef]
55. Chen, J.L.; Kang, S.Z.; Du, T.S.; Guo, P.; Qiu, R.J.; Chen, R.Q.; Gu, F. Modeling relations of tomato yield and fruit quality with water deficit at different growth stages under greenhouse condition. *Agric. Water Manag.* **2014**, *146*, 131–148. [CrossRef]
56. Liu, H.; Li, H.H.; Ning, H.F.; Zhang, X.X.; Li, S.; Pang, J.; Wang, G.S.; Sun, J.S. Optimizing irrigation frequency and amount to balance yield, fruit quality and water use efficiency of greenhouse tomato. *Agric. Water Manag.* **2019**, *226*, 105787. [CrossRef]
57. Adams, S.R.; Cockshull, K.E.; Cave, C.R.J. Effect of temperature on the growth and development of tomato fruits. *Ann. Bot.* **2001**, *88*, 869–877. [CrossRef]
58. Zhang, X.Y.; You, S.Y.; Tian, Y.Q.; Li, J.S. Comparison of plastic film, biodegradable paper and bio-based film mulching for summer tomato production: Soil properties, plant growth, fruit yield and fruit quality. *Sci. Hortic.* **2019**, *249*, 38–48. [CrossRef]
59. Tie, Q.; Hu, H.C.; Tian, F.Q.; Guan, H.D.; Lin, H. Environmental and physiological controls on sap flow in a subhumid mountainous catchment in North China. *Agric. For. Meteorol.* **2017**, *240*, 46–57. [CrossRef]
60. Han, C.; Chen, N.; Zhang, C.K.; Liu, Y.J.; Khan, S.; Lu, K.L.; Li, Y.G.; Dong, X.X.; Zhao, C.M. Sap flow and responses to meteorological about the Larix principis-rupprechtii plantation in Gansu Xinlong mountain, northwestern China. *For. Ecol. Manag.* **2019**, *451*, 117519. [CrossRef]
61. Siddiq, Z.; Chen, Y.J.; Zhang, Y.J.; Zhang, J.L.; Cao, K.F. More sensitive response of crown conductance to VPD and larger water consumption in tropical evergreen than in deciduous broadleaf timber trees. *Agric. For. Meteorol.* **2017**, *247*, 399–407. [CrossRef]
62. Li, L.; Chen, S.W.; Yang, C.F.; Meng, F.J.; Sigrimis, N. Prediction of plant transpiration from environmental parameters and relative leaf area index using the random forest regression algorithm. *J. Clean Prod.* **2020**, *261*, 121136. [CrossRef]
63. Wu, Y.Z.; Zhang, Y.K.; An, J.; Liu, Q.J.; Lang, Y. Sap flow of black locust in response to environmental factors in two soils developed from different parent materials in the lithoid mountainous area of North China. *Trees-Struct. Funct.* **2018**, *32*, 675–688. [CrossRef]
64. Feng, Y.; Cui, N.B.; Du, T.S.; Gong, D.Z.; Hu, X.T.; Zhao, L. Response of sap flux and evapotranspiration to deficit irrigation of greenhouse pear-jujube trees in semi-arid northwest China. *Agric. Water Manag.* **2017**, *194*, 1–12. [CrossRef]
65. Zhang, B.Z.; Xu, D.; Liu, Y.; Li, F.S.; Cai, J.B.; Du, L.J. Multi-Scale evapotranspiration of summer maize and the controlling meteorological factors in north China. *Agric. For. Meteorol.* **2016**, *216*, 1–12. [CrossRef]
66. Xia, G.; Kang, S.; Li, F.; Zhang, J.; Zhou, Q. Diurnal and seasonal variations of sap flow of *Caragana korshinskii* in the arid desert region of north-west China. *Hydrol. Process.* **2008**, *22*, 1197–1205. [CrossRef]
67. Ayyoub, A.; Er-Raki, S.; Khabba, S.; Merlin, O.; Ezzahar, J.; Rodriguez, J.C.; Bahlaoui, A.; Chehbouni, A. A simple and alternative approach based on reference evapotranspiration and leaf area index for estimating tree transpiration in semi-arid regions. *Agric. Water Manag.* **2017**, *188*, 61–68. [CrossRef]
68. Wang, L.; Liu, Z.; Guo, J.; Wang, Y.; Ma, J.; Yu, S.; Yu, P.; Xu, L. Estimate canopy transpiration in larch plantations via the interactions among reference evapotranspiration, leaf area index, and soil moisture. *For. Ecol. Manag.* **2021**, *481*, 118749. [CrossRef]
69. Orgaz, F.; Fernández, M.D.; Bonachela, S.; Gallardo, M.; Fereres, E. Evapotranspiration of horticultural crops in an unheated plastic greenhouse. *Agric. Water Manag.* **2005**, *72*, 81–96. [CrossRef]
70. Papadopoulos, A.P.; Ormrod, D.P. Plant spacing effects on light interception by greenhouse tomatoes. *Can. J. Plant Sci.* **1988**, *68*, 1197–1208. [CrossRef]
71. Qiu, R.J.; Song, J.J.; Du, T.S.; Kang, S.Z.; Tong, L.; Chen, R.Q.; Wu, L.S. Response of evapotranspiration and yield to planting density of solar greenhouse grown tomato in northwest China. *Agric. Water Manag.* **2013**, *130*, 44–51. [CrossRef]
72. Zhang, Z.Z.; Zhao, P.; McCarthy, H.R.; Zhao, X.H.; Niu, J.F.; Zhu, L.W.; Ni, G.Y.; Ouyang, L.; Huang, Y.Q. Influence of the decoupling degree on the estimation of canopy stomatal conductance for two broadleaf tree species. *Agric. For. Meteorol.* **2016**, *221*, 230–241. [CrossRef]
73. Perry, C. Accounting for water use: Terminology and implications for saving water and increasing production. *Agric. Water Manag.* **2011**, *98*, 1840–1846. [CrossRef]
74. Bonachela, S.; Fernandez, M.D.; Cabrera, F.J.; Granados, M.R. Soil spatio-temporal distribution of water, salts and nutrients in greenhouse, drip-irrigated tomato crops using lysimetry and dielectric methods. *Agric. Water Manag.* **2018**, *203*, 151–161. [CrossRef]
75. Buttaro, D.; Santamaria, P.; Signore, A.; Cantore, V.; Boari, F.; Montesano, F.F.; Parente, A. Irrigation Management of Greenhouse Tomato and Cucumber Using Tensiometer: Effects on Yield, Quality and Water Use. *Agric. Agric. Sci. Procedia* **2015**, *4*, 440–444. [CrossRef]
76. Thompson, R.B.; Gallardo, M.; Valdez, L.C.; Fernandez, M.D. Using plant water status to define threshold values for irrigation management of vegetable crops using soil moisture sensors. *Agric. Water Manag.* **2007**, *88*, 147–158. [CrossRef]